Observation of strongly nonquadratic homogeneous upconversion in Er 3+-doped silica fibers and reevaluation of the degree of clustering

Philipsen, Jacob Lundgreen; Broeng, Jes; Bjarklev, Anders Overgaard; Helmfrid, S.; Bremberg, D.; Jaskorzynska, B.; Palsdonir, B.

Published in:
I E E E Journal of Quantum Electronics

Link to article, DOI:
10.1109/3.798101

Publication date:
1999

Document Version
Publisher's PDF, also known as Version of record

Observation of Strongly Nonquadratic Homogeneous Upconversion in Er^{3+}-Doped Silica Fibers and Reevaluation of the Degree of Clustering

Jacob L. Philipsen, J. Broeng, A. Bjarklev, Sten Helmfrid, Dan Bremberg, B. Jaskorzynska, and B. Pálsdóttir

***Abstract*— From careful studies of the 1530-nm fluorescence decay, we obtain the rate of energy transfer upconversion as a function of the inverted population for a series of nine highly Er-doped silica fibers (with concentrations from 0.3 to 8.6 $\cdot$ 10^{25} Er^{3+}-ions per m^3). The results demonstrate that the slow component (microsecond to millisecond scale) of the upconversion, usually referred to as the homogeneous upconversion, is clearly nonquadratic in its dependence on the inverted population, contrary to previous assumptions in the literature. In a second part, we present a new detailed model for energy transfer upconversion, permitting—to our knowledge for the first time—calculation of the rate of migration accelerated upconversion for any given spatial distribution of Er^{3+}-ions. We demonstrate that the results from the decay measurements may be explained with this model. Next, we review the results from a CW green fluorescence detection experiment for the determination of the degree of clustering, which was previously performed on five of the nine fibers. We find accordance between these results and our model, with parameters consistent with those needed to fit the results of the decay experiment, and we arrive at a new conclusion about the nature of clustering.**

***Index Terms*—Erbium materials/devices, integrated optics, integrated optoelectronics, optical amplifiers, optical fiber materials, optical fiber measurements, rare-earth materials/devices.**

I. Introduction

QUENCHING of Er^{3+}-ions by energy transfer upconversion (ETU) is a well-known limiting factor for the performance of high-concentration Er-doped devices. It is among the primary concerns for the realization of Er-doped integrated optical amplifiers and lasers in planar waveguide technology [1]–[3] but also has impact on fiber lasers [4] and amplifiers [5], [6]. Fig. 1 illustrates the two main energy transfer processes taking place between Er^{3+}-ions in optical amplifiers and lasers, namely upconversion and migration [2], [7]. Energy transfer upconversion between two Er^{3+}-ions in the metastable $^4I_{13/2}$ energy level reduces the inverted population by one ion per process, whereas energy migration gives rise to the diffusion of excitation.

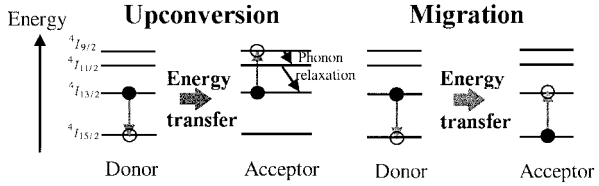

Fig. 1. Energy transfer processes between Er^{3+}-ions.

An important issue in the optimization of material and component design is the distinction [8], [9] between the inevitable contribution to ETU from the homogeneously distributed Er^{3+}-ions and the excess ETU stemming from the clustering of the Er^{3+}-ions, which is to some degree controllable via codoping and the choice of process parameters. The intracluster ETU occurs on a submicrosecond time scale (time constants as short as 50 ns have been measured [10]) due to short interionic distances. The homogeneous upconversion is slower and is usually modeled by a quadratic term in the rate equations [2], [11], [12], which corresponds to assuming that the macroscopic (i.e., averaged over all Er^{3+}-ions) upconversion rate is proportional to the number of Er^{3+}-ions per unit volume in the $^4I_{13/2}$ level: $W_{\mathrm{uc}}(n_2) = C_{\mathrm{uc}} n_2$.

However, we have recently presented modeling results demonstrating that the validity of this quadratic model for a random spatial ion distribution will depend strongly on the relative strength between migration and upconversion [13]. The main goal of this work was to investigate experimentally the validity of the quadratic model. This is done in Sections II and III by measuring and interpreting the decay of the $^4I_{13/2} \rightarrow {}^4I_{15/2}$ 1530-nm fluorescence. In Section IV, we introduce a new model describing ETU for any given spatial distribution of Er^{3+}-ions. The model is used (in Section V) to simulate the experiment and is shown to well explain the nonquadratic behavior of the ETU obtained from the measurements. Finally, in Section VI, we show that reinterpreting earlier performed green fluorescence measurements [9], [14] while using our new model leads to a degree of clustering that differs significantly from what had previously been deduced.

To separate the homogeneous upconversion from the cluster ETU, we study the decay of the 1530-nm fluorescence on a microsecond to millisecond time scale upon the blocking of a pump laser beam, thus avoiding contribution from the

Manuscript received February 23, 1999; revised August 2, 1999. This work was supported in part by the Danish Technical Research Council under the THOR (Technology by Highly Oriented Research) programme, the Swedish Research Council for Engineering Science, and by the Swedish Center for Strategic Research.

J. L. Philipsen, J. Broeng, and A. Bjarklev are with COM Center, Technical University of Denmark, DK-2800 Lyngby, Denmark.

S. Helmfrid, D. Bremberg, and B. Jaskorzynska are with the Laboratory of Photonics and Microwave Engineering, Royal Institute of Technology, S-164 40 Kista, Sweden.

B. Pálsdóttir is with Lucent Technologies Denmark, DK-2605 Brøndby, Denmark.

Publisher Item Identifier S 0018-9197(99)08560-7.

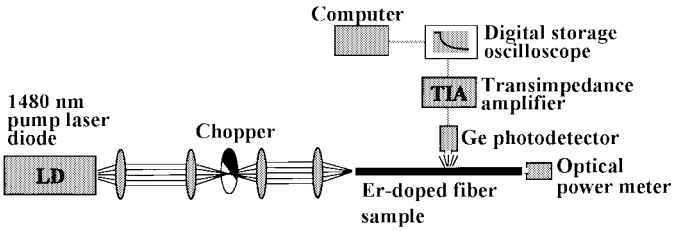

Fig. 2. Experimental setup for measuring 1530-nm fluorescence decay.

ultrafast intracluster ETU. This technique is not new, but, where previous experiments have been interpreted by fitting the measured fluorescence decays to excited state population decays calculated from preassumed models [15]–[17], we wish to take a more basic approach without any *a priori* assumptions about the variation of the upconversion rate with the excited state population.

The decay of the 1530-nm fluorescence power P_{1530} is proportional to the decay of the excited state population n_2, which is governed by $dn_2/dt = -W_{\text{relax}}(n_2)n_2$. Thus, the total relaxation rate, equal to the sum of the spontaneous emission rate and the upconversion rate $W_{\text{relax}}(n_2) = 1/\tau_{\text{rad}} + W_{\text{uc}}(n_2)$, can be determined as

$$W_{\text{relax}} = -\frac{d}{dt}[\ln n_2] = -\frac{d}{dt}[\ln P_{1530}]. \tag{1}$$

Although this idea is very simple, it is not easily carried out, since: 1) fluorescence signals are inherently weak signals and 2) the required numerical differentiation will amplify high-frequency components and thus degrade the signal-to-noise ratio (SNR). Therefore, we had to carry out the experiment in a manner ensuring a large SNR and to carefully optimize the data treatment in order to filter away noise without distorting the final results.

II. Experimental Method

For measuring the 1530-nm fluorescence decay, we used the setup illustrated in Fig. 2. The light from a 100-mW 1480-nm laser diode was focused onto the chopper before being coupled into the Er^{3+}-doped fiber sample under investigation. This allowed us to obtain a fall time below 1 μs for the cutoff of the pump. To detect directly the fluorescence in the 1530-nm band and not the amplified spontaneous emission (ASE), the Ge photodetector was placed transversely to the fiber. (To obtain the maximum possible fluorescence signal, the fiber was attached onto the Ge detector.) Through a transimpedance amplifier and a digital storage oscilloscope, the fluorescence data were acquired by a computer. A second detector was used to monitor the transmitted pump power.

The lengths of the Er^{3+}-doped fiber samples were mainly chosen such that they ensured a suitable amount of scattered pump light. Some scattered pump light was desirable since it provided a well-defined sharp edge (corresponding to the cutoff of the pump) for the oscilloscope to trigger on, whereas too much scattered pump light would saturate the detection system and thus disturb the first part of the fluorescence decay measurement. Since the scattered pump light predominantly originated in an excitation of cladding modes at the incoupling and at the end reflection, a longer fiber (and fluorescence detection sufficiently far from the fiber ends) led to less scattered light. Fiber lengths of 15–20 cm were found to be suitable, when the coating was left on the fibers to increase the stripping of cladding modes. Finally, it was verified that the fiber samples were short enough to avoid any influence from ASE (an elaborate investigation of the influence from ASE was carried out and is described in Section III).

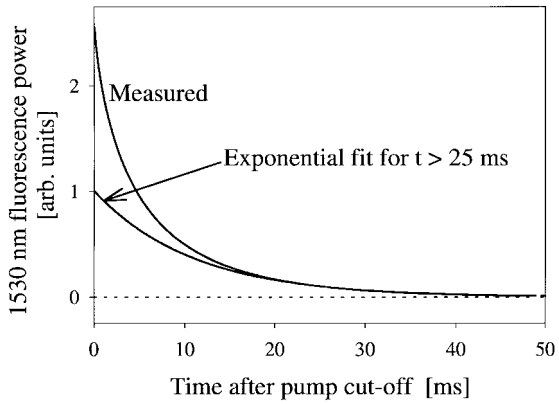

Fig. 3. Decay of the 1530-nm fluorescence for fiber #9, containing $8.6 \cdot 10^{25}$ Er^{3+}-ions per m^3, compared to an exponential fitted to the last 25 ms of the measured decay.

As mentioned in Section I, the calculation of the relaxation rate requires a high SNR on the initial fluorescence data. We therefore applied the feature of the oscilloscope allowing to average over 256 consecutive decays, thus improving the SNR with a factor of about $\sqrt{256} = 16$. Furthermore, we recorded between 120 and 180 of these measurement series on the computer for each Er^{3+}-doped fiber.

III. Processing and Discussion of Experimental Results

Fig. 3 shows an example of a measured fluorescence decay. The decays were sampled by the oscilloscope during 50 ms upon blocking of the pump, with a sampling time of 50 μs. Since 50 μs is much longer than the lifetime of a multiply-excited cluster (cf. Section I), we could—already from the first sample after pump cutoff—consider all clusters to be no more than singly excited. To illustrate the large nonexponential component of the measured decay, we have added an exponential fit to the last 25 ms of the decay.

The 120–180 measurement series for each fiber corresponded to 1–1.5 h of measurement. During this time, there was a risk of decrease in the incoupled pump power, whereas the efficiency for collecting fluorescence by the Ge detector was extremely stable. For each fiber, the data treatment began with an inspection of the ensemble of measured decays, and, in the case of major changes in the incoupled pump power, the involved data were rejected. Furthermore, to compensate for minor changes of pump power in the Er^{3+}-doped fiber, averaging was not done directly on the measured decays, but on the data for the relaxation rate [calculated via (1)] as a function of the inverted population (proportional to the measured fluorescence).

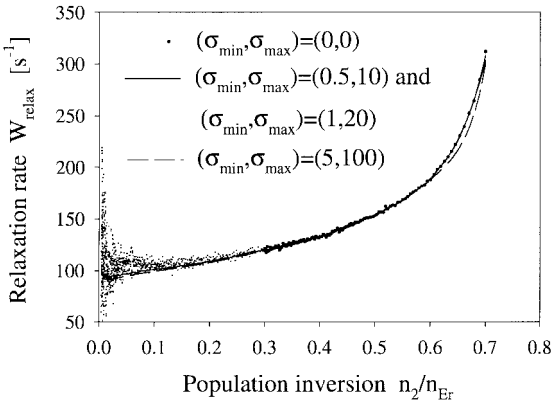

Fig. 4. Optimization of filterwidth for measurements on fiber #6 with an Er^{3+}-concentration of $6.0{\cdot}10^{25}$ ions per m^3. No change is seen between $(\sigma_{\min}, \sigma_{\max}) = (0.5, 10)$ and (1, 20), whereas some distortion sets in at (5, 100). $(\sigma_{\min}, \sigma_{\max}) = (0.5, 10)$ were chosen as appropriate filter parameters.

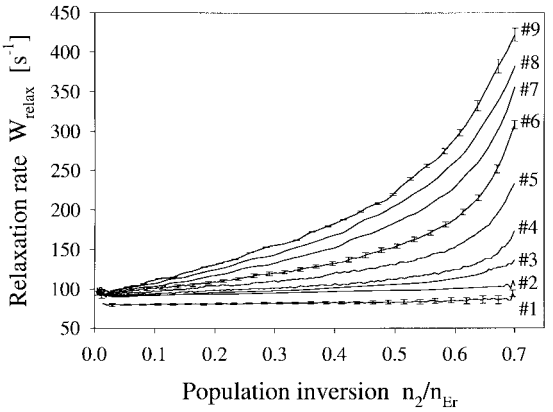

Fig. 5. Relaxation rate from the ${}^4I_{13/2}$ manifold as a function of the population inversion, calculated from the measured 1530-nm fluorescence decays for nine silica fibers (numbered with increasing Er^{3+}-concentration).

The sampled decay sequence $y_{\text{raw}}(m), m = 1, \cdots, M(M \approx 1000)$ must be filtered prior to the numerical differentiation involved in the calculation of the relaxation rate according to (1). A numerical filtering was implemented in the time domain with a Gaussian filter response. A study of the noise related to the measured fluorescence decay revealed a nearly constant noise level, independent of the variation in the signal level, and thus probably dominated by the shot noise related to the detector dark current and to the background light. Consequently, the SNR decreased by approximately 40 dB during the decays, e.g., for fiber #2 (with the second lowest Er^{3+}-concentration: $0.5{\cdot}10^{25}$ ions per m^3), the SNR decreased from around 55 dB to around 15 dB (For fibers with higher Er^{3+}-concentration, the fluorescence signal level was higher and the SNR therefore better.). Since the beginning of the decay signal had a higher content of high-frequency components, whereas the last part of the decay signal was the more noisy, we chose to let the filter width vary with time.

In summary, we performed the convolution

$$y_{\text{filtered}}(m) = \sum_{k=-K(m)}^{k=K(m)} h(k; m) y_{\text{raw}}(m-k) \qquad (2)$$

with $K(m) = \min\{m-1, M-m\}$ (symmetric truncation near the ends to avoid boundary effects) and with the time-varying filter impulse response

$$h(k; m) = \frac{\exp\left(-\dfrac{k^2}{2\sigma^2(m)}\right)}{\displaystyle\sum_{k=-K(m)}^{k=K(m)} \exp\left(-\frac{k^2}{2\sigma^2(m)}\right)} \qquad (3)$$

where $\sigma(m)$ is a linearly growing function. The minimum and maximum filterwidth $\sigma_{\min} = \sigma(1)$ and $\sigma_{\max} = \sigma(M)$, respectively, were optimized for each measurement series by observing at which filterwidths the final result, $W_{\text{relax}}(n_2)$ became distorted. This procedure is illustrated in Fig. 4 for the measurements on fiber #6. For this measurement series, calculation of the relaxation rate was possible without any filtering (shown with dots on the figure), but for other measurement series, some filtering was necessary to get any sensible results at all.

Comparison between the $W_{\text{relax}}(n_2)$-curves calculated from the 120–180 measurement series per fiber showed excellent agreement, except for the cases with major changes in the incoupling of pump power, leading to, e.g., triggering errors. As expected, measurements following a minor decrease in the incoupled pump power led to $W_{\text{relax}}(n_2)$-curves that coincided perfectly with the previous measurements, but were truncated at high values of the inverted population n_2. Finally, for some fiber samples, measurements were repeated after several days, and perfect reproducibility was again observed.

Fig. 5 summarizes the measurements on all nine fibers, showing the relaxation rate for the Er^{3+}-ions in the ${}^4I_{13/2}$ level as a function of the population inversion n_2/n_{Er}. For each fiber, the curve represents an average over the performed measurement series. Due to lack of space, error bars indicating the standard deviations are only shown for three of the curves. The fluorescence power only yields a relative measurement of the inverted population. Prior to all measurement series, we measured the fluorescence power as a function of the pump power, and saturation was observed in all cases. Comparison of the saturation curves with a simple model (not including ETU) gave values around 0.7 for the inversion at full pump power (the maximum obtainable inversion with 1480-nm pumping was calculated to be 0.75 on the basis of emission and absorption spectra). We thus chose to normalize the inversion to 0.7 at the beginning of all decays, but we must emphasize that the absolute scale for the population inversion is only approximate and that, in particular for the fibers with the highest Er-concentration, the actual inversion may be significantly lower.

We see from Fig. 5 that fibers #2–9, which are aluminosilicate fibers, all have a relaxation rate of approximately 90 s^{-1} in the limit of zero inversion, corresponding to a radiative lifetime around 11 ms. Fiber #1 is a germanosilicate fiber and has a radiative lifetime of 12.6 ms. The increase in the relaxation rate with the inverted population demonstrates the quenching of the Er^{3+}-ions, and we shall assume this quenching to be dominated by energy transfer upconversion

between Er^{3+}-ions. This assumption is supported by numerous observations reported in the literature [1], [8], [9], [11] together with the fact that we were able to detect a significant 980-nm fluorescence signal when approaching a Si detector to the fibers (ETU leads to 980-nm fluorescence from the $^4I_{11/2}$ level, whereas this is not the case for quenching mechanisms involving the transfer of energy from an Er^{3+}-ion to, e.g., an OH^--ion). Finally, the fact that the quenching rate grows with both the Er-concentration and the population inversion also supports the assumption of ETU as the dominating quenching mechanism.

The main conclusion from Fig. 5 is that the upconversion rate $W_{\rm uc} = W_{\rm relax} - 1/\tau_{\rm rad}$ experienced by the Er^{3+}-ions in the $^4I_{13/2}$ manifold does *not* grow linearly with the $^4I_{13/2}$ population, i.e., the model predicting a quadratic dependence of the number of ETU processes on the excited state population, does not hold for our fibers. On the contrary, the curves all bend upwards, as would be expected for the case, where migration is too weak for the quadratic model to be valid [13]. At first sight, the tendency of bending upwards seems stronger for the curves representing the highest concentration fibers, but a closer inspection (comparison of the curves with the maximum upconversion rate normalized to 1) reveals that, apart from fibers #1 and #2, where the results are too noisy, all the curves have roughly the same shape.

To confirm our conclusion, we must verify that ASE did not affect the results. Due to the transverse detection setup, ASE did not contribute directly to the detected signal, but Er^{3+}-transitions $^4I_{13/2} \rightarrow {}^4I_{15/2}$ stimulated by ASE might accelerate the beginning of the $^4I_{13/2}$ population decay and thus be the real cause for the upwards bending of the curves for the relaxation rate. To exclude this possibility, we repeatedly measured the fluorescence decay from fiber #6 ($6.0{\cdot}10^{25}$ Er^{3+}-ions per m^3) while gradually reducing the fiber length from 50 to 2 cm. Fig. 6 shows a superposition of the obtained curves for the relaxation rate as a function of the inversion, together with the maximum relaxation rate as a function of the fiber length. We see that all the curves for the relaxation rate bend upwards, so this effect is not merely a result of ASE. On the other hand, there is a significant spread in the maximum relaxation rate, which we attribute to two factors in the experimental conditions: 1) we only recorded one measurement for each fiber length, and the statistical uncertainty is, therefore, larger than for the results in Fig. 5, and 2) the pump incoupling was not readjusted after each cutback (the points where $W_{\rm relax,\,max}$ grows with decreasing fiber length match with the reoptimizations of the incoupling).

To remove any remaining doubt, we construct a simple model of the influence from ASE. Assuming constant population inversion along the fiber (this assumption, although simplistic, will not change the order of magnitude for the ASE), the spectral density of forward propagating ASE at distance z from the pump incoupling becomes [18]

$$S^+_{\rm ASE}(\nu, z) = \frac{2h\nu\gamma_{\rm em}}{\gamma_{\rm em} - \gamma_{\rm abs}} \left(\exp[(\gamma_{\rm em} - \gamma_{\rm abs})z] - 1\right). \quad (4)$$

In this expression, $\gamma_{\rm em}(\nu) = \sigma_{\rm em}(\nu)\Gamma n_2$ and $\gamma_{\rm abs}(\nu) = \sigma_{\rm abs}(\nu)\Gamma(n_{\rm Er} - n_2)$, where $\sigma_{\rm em}$ and $\sigma_{\rm abs}$ are the emission and absorption cross sections for the $^4I_{15/2} \leftrightarrow {}^4I_{13/2}$ transition, ν is the optical frequency, Γ is the confinement factor, $n_{\rm Er}$ and n_2 are, respectively, the total concentration of Er^{3+}-ions and the concentration of Er^{3+}-ions excited to the $^4I_{13/2}$ level, and h is Planck's constant. The expression for the backward ASE is obtained from (4) by replacing z by $L - z$, where L is the fiber length.

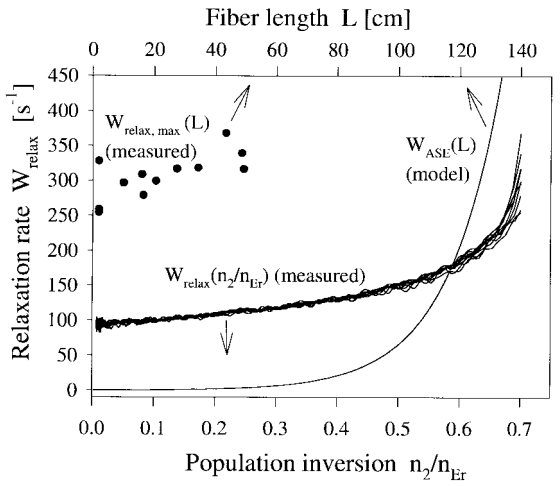

Fig. 6. Results of experimental investigation of the impact of fiber length on the measured relaxation rate, for fiber #6 with an Er^{3+}-concentration of $6.0{\cdot}10^{25}$ ions per m^3. The figure furthermore shows the calculated net rate of ASE stimulated relaxation at an inversion of 0.7 as a function of fiber length, also for fiber #6.

The ASE will imply a net relaxation rate on the Er^{3+}-ions, given as the difference between the number of ASE stimulated emission and absorption processes per time divided by the $^4I_{13/2}$ population. For this net relaxation rate, we arrive at the following expression (where a_d is the doping radius):

$$W^{\rm ASE}_{\rm relax}(z, n_2) = \frac{2}{\pi a_d^2 n_2} \int_0^\infty \gamma_{\rm em}(\nu)(\exp[(\gamma_{em} - \gamma_{\rm abs})z] + \exp[(\gamma_{\rm em} - \gamma_{\rm abs})(L - z)] - 2)\, d\nu. \quad (5)$$

In Fig. 6, we have shown the calculated net rate of ASE stimulated emission for fiber #6 at an inversion of 0.7 as a function of the fiber length. To obtain a worst case prediction, the fiber end was used as calculation point. We see that, for a fiber shorter than around 50 cm, the ASE stimulated emission rate is negligible and, thus, it cannot have had any influence on the measurements performed at fiber lengths of 15–20 cm. We have performed these calculations for all 9 fibers and have verified that the ASE stimulated emission rates are negligible compared to the measured upconversion rates in all cases.

We can equally exclude scattered ASE entering the transverse detector together with the fluorescence as an error source. Since the net rate of ASE stimulated emission is negligible compared to the spontaneous emission rate, the number of ASE photons generated per time is thus negligible compared to the number of emitted fluorescence photons per time. Also, the number of scattered ASE photons per time must be smaller than the number of generated ASE photons per time in order for the ASE to experience a net gain.

IV. Continuum Model for ETU

In [13], we presented a detailed model for calculation of the macroscopic upconversion rate from an assumed microscopic spatial distribution of the Er^{3+}-ions together with an assumed dependence of the upconversion and migration probabilities on the interionic distance. In a first version of the model, we used Monte Carlo simulations to generate the Er^{3+} sites as well as to simulate the temporal behavior of the ions, whereas a second version described the temporal behavior via equations for the excitation probabilities for each ion together with the joint excitation probabilities for neighboring ions. The second version was much faster than the first, but still demanded very long calculation times to obtain an adequate statistical certainty. For this reason, we limited ourselves to consideration of the dipole–dipole interaction between randomly distributed Er^{3+} ions.

In this paper, we present a new model based on equations for the probability densities of the second-order spatial ion distributions, eliminating the stochastical element in the calculations and allowing a reduction in calculation times by many orders of magnitude (typically from days to minutes). As in [13], we consider only the populations of the ground level $^4I_{15/2}$ and the first excited level $^4I_{13/2}$. We let $f^{**}(r, t)$ designate the probability (at time t) per (unit volume)^2 of finding two excited Er^{3+}-ions with a distance r between them. Similarly, we introduce the distribution f^{*o} of nonexcited Er^{3+}-ions relative to excited Er^{3+}-ions, the distribution f^{oo} of nonexcited Er^{3+}-ions relative to nonexcited Er^{3+}-ions, and the distribution f^{Er} of all Er^{3+}-ions relative to all Er^{3+}-ions. Since $f^{\mathrm{Er}} = f^{**} + 2f^{*o} + f^{oo}$, the distribution f^{oo} may be eliminated. The limiting values of the distributions are related to the population concentrations, since ions sufficiently far apart do not interact

$$\begin{aligned}\lim_{r\to\infty} f^{**}(r, t) &= n_2^2(t)\\ \lim_{r\to\infty} f^{oo}(r, t) &= n_1^2(t)\\ \lim_{r\to\infty} f^{*o}(r, t) &= n_1(t)n_2(t)\\ \lim_{r\to\infty} f^{\mathrm{Er}}(r) &= n_{\mathrm{Er}}^2. \end{aligned} \tag{6}$$

The impact of absorption (with rate W_{abs}), emission (with rate W_{em}), and ETU processes on the temporal evolution of the second-order distributions f^{**} and f^{*o} can be expressed in terms of the third-order distributions, and, by applying appropriate approximations to these, one obtains the following system of equations:

$$\begin{aligned}\frac{\partial f^{**}(r,t)}{\partial t} &= -\left(2W_{\mathrm{em}}(t) + P_{\mathrm{uc}}(r) + 2W_{\mathrm{uc}}(t)\right)f^{**}(r, t)\\ &\quad + 2W_{\mathrm{abs}}(t)f^{*o}(r, t)\\ \frac{\partial f^{*o}(r,t)}{\partial t} &= -\left(3W_{\mathrm{abs}}(t) + W_{\mathrm{em}}(t) + W_{\mathrm{uc}}(t)\right)f^{*o}(r, t)\\ &\quad + \left(-W_{\mathrm{abs}}(t) + W_{\mathrm{em}}(t) + \frac{1}{2}P_{\mathrm{uc}}(r) + W_{\mathrm{uc}}(t)\right)\\ &\quad \cdot f^{**}(r, t) + W_{\mathrm{abs}}(t)f^{\mathrm{Er}}(r)\end{aligned} \tag{7}$$

where $P_{\mathrm{uc}}(r)$ is the probability per time unit for two excited Er^{3+}-ions at distance r to perform ETU and where the macroscopic upconversion rate is given as the number of upconversion processes per time and volume unit divided by the excited state population concentration

$$W_{\mathrm{uc}}(t) = \frac{N_{\mathrm{uc}}(t)}{n_2(t)} = \frac{1}{2n_2(t)}\int_0^\infty P_{\mathrm{uc}}(r)f^{**}(r, t)4\pi r^2\,dr. \tag{8}$$

We have verified that (6)–(8) lead to results in accordance with those obtained by our previously reported stochastical simulations, when energy migration is excluded. When trying to include migration into (7), it turns out not to be possible to eliminate the third-order distributions. We therefore choose a more phenomenological description of the impact of migration on the spatial distributions. The number of migration processes per time and volume unit can be expressed as

$$N_{\mathrm{mig}}(t) = \int_0^\infty P_{\mathrm{mig}}(r)f^{*o}(r, t)4\pi r^2\,dr \tag{9}$$

where $P_{\mathrm{mig}}(r)$ is the probability per time unit for an excitation to migrate between two Er^{3+}-ions at distance r. We note that the Er^{3+}-ions in the ground level will experience an average migration-induced excitation rate of $W_{\mathrm{mig}\uparrow}(t) = N_{\mathrm{mig}}(t)/n_1(t)$, whereas the excited Er^{3+}-ions will experience an average relaxation rate of $W_{\mathrm{mig}\downarrow}(t) = N_{\mathrm{mig}}(t)/n_2(t)$ caused by energy migration. We therefore simply add $W_{\mathrm{mig}\uparrow}$ and $W_{\mathrm{mig}\downarrow}$ to, respectively, the absorption and emission rate. This approximation will lead to an overestimation of the impact of migration on the spatial distributions f^{**} and f^{*o}, since it does not take into account that two closely spaced Er^{3+}-ions—working as a quenching center—will tend to deplete a zone around them from excitation and therefore will have less probability of being excited by energy migration. However, we have, through comparison with our stochastical simulations, verified that the correct macroscopic results may be obtained by applying a value for the strength of migration that is smaller than the physical parameter value.

As input to the model, we need to specify the distribution of Er^{3+}-ions, $f^{\mathrm{Er}}(r)$, together with the dependencies $P_{\mathrm{uc}}(r)$ and $P_{\mathrm{mig}}(r)$ of upconversion and migration probabilities on the interionic distance. We shall assume that $f^{\mathrm{Er}}(r)$ is a superposition of a homogeneous distribution with a certain minimum distance R_{min} between the Er^{3+}-ions and a narrow peak around a distance R_{cl} slightly smaller than R_{min}, representing the sites leading to clustering

$$f^{\mathrm{Er}}(r) = n_{\mathrm{Er}}^2\Theta(r - R_{\mathrm{min}}) + \alpha_{\mathrm{cl}}f_{\mathrm{cl}}(r). \tag{10}$$

Here, Θ is the Heavyside unity function, and f_{cl} is a narrow Gaussian, centered around R_{cl}, and normalized so that α_{cl} becomes the average excess number of Er^{3+}-neighbors that each Er^{3+}-ion has due to clustering. A physically more interesting parameter is the fraction k_{unbl} of the Er^{3+}-ions that are unbleachable due to clustering. Thus, the cluster-induced reduction of the maximum obtainable gain (in dB) of an amplifier is given by the factor $1 - k_{\mathrm{unbl}}(1 + \sigma_{\mathrm{abs}}/\sigma_{\mathrm{em}})$, where σ_{abs} and σ_{em} are the absorption and emission cross sections at the signal wavelength. The relation between α_{cl} and k_{unbl} depends slightly on the distribution of cluster

sizes. If all clusters were pairs, $k_{\rm unbl} = \alpha_{\rm cl}/2$, since only one ion per pair can be inverted. Actually, considering only the second-order ion distributions in the way the model does corresponds to implicitly assuming a near-Poissonian distribution of cluster sizes. From (7), it can be shown that the fraction of unbleachable Er^{3+}-ions in the model is $k_{\rm unbl} = \alpha_{\rm cl}/2 + 1 - \sqrt{1+(\alpha_{\rm cl}/2)^2}$. This relation allows us to relate the external parameter $k_{\rm unbl}$ to the internal parameter $\alpha_{\rm cl}$ in the model.

Several X-ray absorption fine structure (XAFS) measurements with the purpose of studying the local environment around Er^{3+} in various host glasses have been reported [19], [20]. These studies generally show: 1) a coordination shell of six O-atoms at a distance around 0.22–0.23 nm from the Er-atom followed by 2) a coordination shell with Si-atoms at a distance around 0.31 nm in the case of silica, but no sign of neighboring Er-atoms within the 0.4-nm range of the XAFS method has been reported. Thus, neither the location $R_{\rm cl}$ nor the shape of the assumed cluster peak in the ion distribution is known. However, it is known that the timescale of the intracluster ETU is much faster than the timescale of our measurements. Therefore, we set $P_{\rm uc}(r) = 1/\tau_{\rm cl}$ with $\tau_{\rm cl} = 1$ μs (having verified that the modeling results do not depend on $\tau_{\rm cl}$ for $\tau_{\rm cl}$ less than a few microseconds) for all r under the cluster peak, and thus only the area under the cluster peak counts. We arbitrarily set $R_{\rm cl} = 0.5$ nm.

For interaction outside clusters, we shall consider only the dipole–dipole terms [13], [21]

$$P_{\rm uc}(r) = \frac{1}{\tau_{\rm rad}}\left(\frac{R_{\rm uc}}{r}\right)^6$$
$$P_{\rm mig}(r) = \frac{1}{\tau_{\rm rad}}\left(\frac{\tilde{R}_{\rm mig}}{r}\right)^6 \qquad (11)$$

where ˜ is to indicate that the migration strength parameter in our model is a phenomenological parameter whose value will differ from the physical value. We choose to assume the minimum distance $R_{\rm min} = 0.6$ nm for the homogeneous part of the Er^{3+}-ion distribution, noting that a wrong value will just correspond to a scaling of the parameters $R_{\rm uc}$ and $\tilde{R}_{\rm mig}$.

To illustrate the model, Fig. 7 shows the distribution $f^{\rm Er}$ given by (10) for the case $k_{\rm unbl} = 5\%$ together with calculated steady-state solutions for the distributions f^{**} and f^{*o} for different values of the migration strength parameter $\tilde{R}_{\rm mig}$. As expected, ETU creates a spatial hole burning phenomenon in the distribution f^{**} and a corresponding bump in the distribution f^{*o}. Energy migration tends to bring the distributions back toward the shape of the distribution $f^{\rm Er}$ of all Er^{3+}-ions.

V. Comparison Between Model and Experiment

To simulate the experimental conditions of our fluorescence decay measurements, we first set $W_{\rm abs}(t) = W_{\rm pump}^{1480}$ and $W_{\rm em}(t) = W_{\rm pump}^{1480}\sigma_{\rm em}$ (1480 nm)/$\sigma_{\rm abs}$ (1480 nm)+$1/\tau_{\rm rad}$, where $W_{\rm pump}^{1480}$ is the pump absorption rate, and determine the steady-state solution to (7). We then set $W_{\rm abs}(t) = 0$ and $W_{\rm em}(t) = 1/\tau_{\rm rad}$ and find the temporal evolution of the distributions f^{**} and f^{*o}, which allows us to calculate

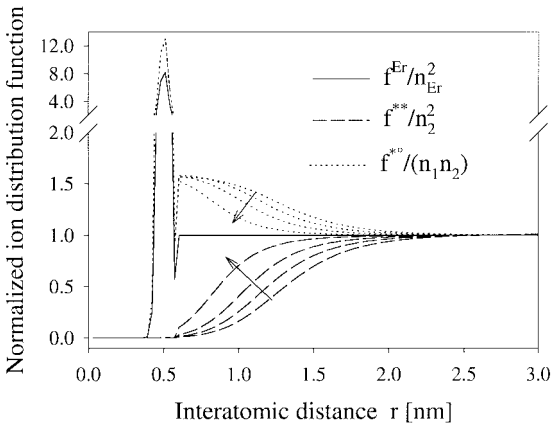

Fig. 7. Modeling of the second-order spatial Er^{3+}-ion distributions for a glass with an Er^{3+}-concentration of $n_{\rm Er} = 5 \cdot 10^{25}$ m^{-3} and a degree of clustering given by $k_{\rm unbl} = 5\%$. The distributions f^{**} and f^{*o} are shown under stationary conditions at an inversion of $n_2/n_{\rm Er} = 0.6$ and are calculated for an upconversion strength parameter of $R_{\rm uc} = 2.0$ nm and with a migration strength parameter growing in the direction of the arrows ($\tilde{R}_{\rm mig} = 0,\ 1.2,\ 1.5$, and 2.0 nm).

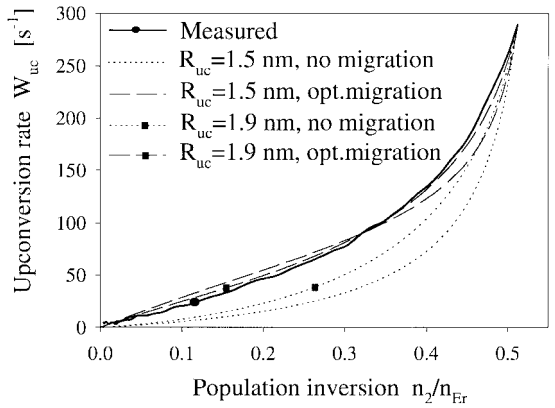

Fig. 8. Fitting of the continuum model to fluorescence decay experiment for fiber #8 ($8.6{\cdot}10^{25}$ Er^{3+}-ions per m^3). For each of the considered $R_{\rm uc}$-values, the calculated curves for no migration (dotted lines) and optimized migration (dashed lines) are shown. The population inversion (which is only measured relatively in the experiment) has for all the curves shown been scaled to the population inversion predicted by the model when using the parameter choice leading to the least square fit between model and experiment ($R_{\rm uc} = 1.9$, $\tilde{R}_{\rm mig} = 0.98$ nm).

the excited state population and the average upconversion rate $W_{\rm uc}$ as functions of time. We use the $W_{\rm uc}(n_2)$-curves as the basis for comparing model and experiment.

To fit the model to the experimental data, we begin by assuming no clustering, i.e., $k_{\rm unbl} = 0$. We then assume a value of $R_{\rm uc}$ and adapt the pumping rate so that the measured and calculated $W_{\rm uc}(n_2)$-curves coincide at the maximum inversion. Then, $\tilde{R}_{\rm mig}$ is varied until the best fit between the two curves is obtained. Fig. 8 illustrates this process for fiber #8 ($8.6{\cdot}10^{25}$ Er^{3+}-ions per m^3) for the cases $R_{\rm uc} = 1.5$ nm and $R_{\rm uc} = 1.9$ nm. It is clear from this figure that $R_{\rm uc} = 1.9$ nm leads to a good fit, whereas the fit is poor for $R_{\rm uc} = 1.5$ nm. By demanding that the sum of the square of the residuals should not exceed twice its minimum value, we are able to determine $R_{\rm uc}$ and $\tilde{R}_{\rm mig}$ within certain intervals. However, these intervals could have been significantly narrower if we

TABLE I
RADIATIVE LIFETIME AND MAXIMUM UPCONVERSION RATE AS MEASURED IN THE FLUORESCENCE DECAY EXPERIMENT, TOGETHER WITH UPCONVERSION AND MIGRATION STRENGTH PARAMETERS OBTAINED BY FITTING TO THE CONTINUUM MODEL

Fibre no.	Glass type	$[Er^{3+}]$ [ions/m^3]	Co-doping	τ_{rad}	W_{uc}^{max}	R_{uc}	$\tilde{R}_{mig}$
#1	Germano-silicate	$0.3 \cdot 10^{25}$	-	12.6 ms	8.6 s^{-1}	-	-
#2	Alumino-silicate	$0.5 \cdot 10^{25}$	La	11.0 ms	12.3 s^{-1}	-	-
#3		$2.4 \cdot 10^{25}$	La	11.2 ms	47.6 s^{-1}	1.7 ±0.1 nm	1.15±0.15 nm
#4		$2.8 \cdot 10^{25}$	La	11.0 ms	82.4 s^{-1}	1.55±0.05 nm	1.11±0.05 nm
#5		$4.4 \cdot 10^{25}$	La	10.9 ms	141.9 s^{-1}	1.67±0.07 nm	0.97±0.05 nm
#6		$6.0 \cdot 10^{25}$	La	10.8 ms	215.4 s^{-1}	1.65±0.05 nm	0.95±0.05 nm
#7		$8.0 \cdot 10^{25}$	La	10.9 ms	264.1 s^{-1}	1.85±0.15 nm	0.95±0.05 nm
#8		$8.6 \cdot 10^{25}$	La	10.8 ms	289.0 s^{-1}	1.9 ±0.1 nm	0.98±0.03 nm
#9		$8.6 \cdot 10^{25}$	-	11.0 ms	331.3 s^{-1}	2.1 ±0.2 nm	1.01±0.04 nm

had measured the fluorescence rise time, since the pumping rate could have been deduced from this ($1/\tau_{rise} = W_{pump}^{1480} + 1/\tau_{rad}$). Instead, we can only give a lower limit for W_{pump}^{1480} based on a measurement of the residual pump power at the end of the Er-doped fiber. Using this lower limit, the intervals for R_{uc} and $\tilde{R}_{mig}$ can be narrowed slightly.

Finally, we vary the cluster parameter k_{unbl}, which turns out not to have any impact on the fitting of the model to the experimental $W_{uc}(n_2)$-curves. Thus, we can conclude that reactivation of clusters through energy migration had negligible influence on our decay experiment, which therefore cannot be used to quantify clustering.

The fitting was carried out for all the fibers except for #1 and #2 where the SNR for the $W_{uc}(n_2)$-curve was too bad for any fitting to be meaningful. (This was a consequence of the weak fluorescence signal combined with a small upconversion rate compared to τ_{rad}, both of which were due to a lower Er-concentration than in other fibers.) For all other fibers, a good fit between the experiment and model was obtained. The results from the decay experiment and the fitting to the model are summarized in Table I.

VI. REINTERPRETATION OF THE GREEN FLUORESCENCE EXPERIMENT

In order to quantify the degree of clustering, a different type of experiment must be made. One of the standard methods is a green fluorescence detection experiment, first described in [9]. We have previously reported on the characterization of five of the fibers discussed in this paper (fibers #2, 3, 5, 8, and 9) by this method [14]. In this experiment, we pumped a short sample (~1 cm) of the Er-doped fiber with up to 275 mW of pump power from a Ti : sapphire laser and observed the steady-state powers of the infrared fluorescence around 1530 nm and the green fluorescence around 540 nm as functions of pump power. The 1530-nm fluorescence provides a measurement of the population n_2 of the metastable $^4I_{13/2}$ level, whereas the green fluorescence power divided by the pump power is proportional to the population n_3 of the $^4I_{11/2}$ manifold, since excited-state absorption from this level is the source of the green fluorescence. The populations n_2 and n_3 were then fitted to a simple model in order to extract the fraction k_{unbl} of unbleachable Er^{3+}-ions and an effective lifetime τ_x for these ions. The results showed heavy clustering with k_{unbl} growing strongly with the Er-concentration from 1% for fiber #2 to 23% for fiber #8 and then further to 42% for fiber #9, which has the same Er-concentration as #8, but contains no lanthanum. Very long effective lifetimes τ_x were found, growing from around 50 μs for fiber #2 to around 400 μs for fiber #8, indicating influence from homogeneous upconversion and migration.

In order to reinterpret the results from the green fluorescence experiment, we need to enable the continuum model to predict also the $^4I_{11/2}$ population n_3. To do this, we use a perturbation type approach. Since $n_3 \ll n_2$ due to the short lifetime (around 10 μs [22]) of the $^4I_{11/2}$ manifold, we assume that the $^4I_{13/2}$ level population n_2 and the macroscopic upconversion rate W_{uc} are correctly predicted by the 2-level model. The $^4I_{11/2}$ population may then by demanding $dn_3/dt = 0$ be found as

$$n_3 = \frac{W_{pump}^{980}(n_{Er} - n_2) + W_{uc} n_2}{W_{pump}^{980} + \dfrac{1}{\tau_{11/2}}} \tag{12}$$

where W_{pump}^{980} is the pump absorption rate and $\tau_{11/2}$ is the $^4I_{11/2}$ lifetime, which we set to 10 μs. To simulate the 980-nm pumping, we set $W_{abs}(t) = W_{pump}^{980}$ and $W_{em}(t) = 1/\tau_{rad}$ in the continuum model.

To fit our model to the results from the green fluorescence experiment, we use the values of R_{uc} and $\tilde{R}_{mig}$ that were extracted from the decay experiment. We then adjust the proportionality constant between pump power and pump rate so that model and experiment agree with respect to the shape of the n_2 versus pump power curve. Finally, we fit for the shape of the n_3 versus pump power curve to determine k_{unbl}. Fig. 9 illustrates the last step of this procedure for the fiber #8 ($8.6 \cdot 10^{25}$ Er^{3+}-ions per m^3). For this fiber, we clearly get the best fit for $k_{unbl} \approx 0$.

For all the fibers #3, 5, 8, and 9, we obtain accordance between the continuum model and the results from the green fluorescence experiment, when using the values of R_{uc} and $\tilde{R}_{mig}$ found from the decay experiment. For each fiber, both extremes of the determined intervals for R_{uc} and $\tilde{R}_{mig}$ have been tried. Table II compares the previously reported and the new interpretation of the green fluorescence experiment.

We see that there is a dramatic difference in the extracted values for the fraction k_{unbl} of Er^{3+}-ions that are unbleachable due to clustering. According to the new model, only fiber

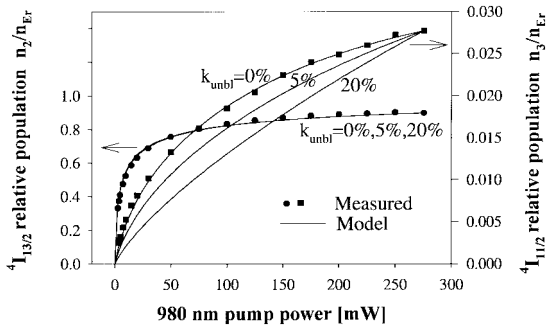

Fig. 9. Fitting of continuum model to green fluorescence experiment for fiber #8 ($8.6{\cdot}10^{25}$ Er^{3+}-ions per m^3). The populations n_2 and n_3 (which are only measured on their relative scales in the experiment) have, for all the curves shown, been scaled to fit at maximum pump power with the populations predicted by the model when using $k_{\mathrm{unbl}} = 0$. Thus, n_3 in the model actually *grows* with the assumed value of k_{unbl}, contrary to what appears in the figure.

TABLE II
COMPARISON OF CLUSTER PARAMETERS OBTAINED FROM THE GREEN FLUORESCENCE EXPERIMENT BY FITTING WITH, RESPECTIVELY, THE SIMPLE MODEL AND THE NEW, DETAILED CONTINUUM MODEL

Fibre no.	$[Er^{3+}]$ [ions/m^3]	Co-doping	Interpretation with simple model		Interpretation with new model
			k_{unbl}	τ_x	k_{unbl}
#3	$2.4 \cdot 10^{25}$	La	8.5 %	177 μs	1 %
#5	$4.4 \cdot 10^{25}$	La	13 %	193 μs	2 %
#8	$8.6 \cdot 10^{25}$	La	23 %	388 μs	0 %
#9	$8.6 \cdot 10^{25}$	-	42 %	128 μs	7-10 %

#9, which contains no lanthanum codoping, shows significant clustering. However, when comparing the two interpretations, it is important to remember that in the continuum model the homogeneous part of the Er^{3+}-ion distribution also contains ions with a very short lifetime due to ETU (with the values for R_{uc} from Table I and with $R_{\mathrm{min}} = 0.6$ nm: lifetimes down to a few microseconds). What the new interpretation may tell us is that there is very little *excess* clustering compared to what a purely homogeneous distribution would have given. This corresponds to what was concluded in [9] for some of the fibers investigated.

On the other hand, we see from Table I that the values of the upconversion strength parameter R_{uc}, determined from the decay experiment, grow with the Er-concentration from $R_{\mathrm{uc}} \approx 1.55$ nm for fiber #4 to $R_{\mathrm{uc}} \approx 2.1$ nm for fiber #9. Remembering that the upconversion probability is proportional to the sixth power of R_{uc} and that this parameter should actually be concentration independent, we conclude that these figures are hiding a physical phenomenon not included in our model. The results indicate that the Er^{3+}-ion distribution *does* in fact change with concentration, but primarily in a manner preserving its homogeneous type shape. We propose that the clustering is not due to a well-defined distinct site for one Er^{3+}-ion near another Er^{3+}-ion, but rather to a smeared out site, leading to a broad cluster peak in the distribution f^{Er}, detectable in both a steady state as well as in a decay experiment. This would also explain why an Er–Er peak has not been observed in any XAFS study of Er-doped glasses.

We finally note that, even for the low concentration fibers, the found values for R_{uc} are very large compared to the predicted values around 1 nm, calculated from the overlap integral between the $^4I_{13/2} \rightarrow {}^4I_{15/2}$ emission spectrum and the $^4I_{13/2} \rightarrow {}^4I_{9/2}$ excited state absorption spectrum [2], [13]. The reason for this may be that higher order terms representing dipole–quadrupole and quadrupole–quadrupole interactions are not negligible and should have been included in (11). (Inclusion of such terms would not have changed our conclusions, since this would not change the concentration dependencies in the model.) Another possible explanation for the large R_{uc} values is that only the ratio $R_{\mathrm{uc}}/R_{\mathrm{min}}$ is actually determined, cf. Section IV. If the physical R_{min} is smaller than the assumed 0.6 nm, the actual R_{uc} will be correspondingly smaller than the value listed in Table I. Since the XAFS studies reported in the literature only rule out *distinct* peaks in the distribution f^{Er}, R_{min} might even be smaller than the XAFS range limit of 0.4 nm.

VII. CONCLUSION

From a 1530-nm fluorescence decay measurement on a series of silica fibers, we have demonstrated that the slow component of the energy transfer upconversion does not obey the quadratic law usually assumed for homogeneous upconversion. We have developed a model based on equations for the second-order spatial distributions of excited and nonexcited Er^{3+}-ions, which can explain our experimental results.

By fitting our model to both the decay experiment and to a previously reported green fluorescence detection experiment, we have demonstrated that, as the Er-concentration grows in the examined fibers, we get increased energy transfer upconversion, not in the form of an increased ultrafast cluster contribution, but more taking the form of an increased homogeneous upconversion, with both fast and slow components. This indicates the presence of a clustering phenomenon with a broad interval of Er^{3+}-Er^{3+} distances.

We furthermore conclude that the green fluorescence experiment is a useful tool for obtaining quantitative information about the ETU in an Er-doped material, but is not fit for determining the fraction of unbleachable (fast decaying) Er^{3+}-ions. For this, one should rather turn to direct observation through nanosecond spectroscopy [23].

REFERENCES

[1] G. Nykolak, P. C. Becker, J. Shmulovich, Y. H. Wong, D. J. DiGiovanni, and A. J. Bruce, "Concentration-dependent $^4I_{13/2}$ lifetimes in Er^{3+}-doped fibers and Er^{3+}-doped planar waveguides," *IEEE Photon. Technol. Lett.,* 1993.

[2] M. Hempstead, J. E. Román, C. Ye, J. S. Wilkinson, P. Camy, P. Laborde, and C. Lerminiaux, "Anomalously high uniform upconversion in an Erbium-doped waveguide amplifier," in *Proc. 7th Eur. Conf. Integrated Optics (ECIO'95),* 1995, pp. 233–236, paper TuC4.

[3] D. Barbier, "Performances and potential applications of Erbium doped planar waveguide amplifiers and lasers," in *Optical Amplifiers and Their Applications (OAA'97),* Victoria, B.C., Canada, July 1997.

[4] J. L. Wagener, P. F. Wysocki, M. J. F. Digonnet, H. J. Shaw, and D. J. DiGiovanni, "Effects of concentration and clusters in Erbium-doped fiber lasers," *Opt. Letters,* vol. 18, no. 23, pp. 2014–2016, 1993.

[5] N. Kagi, A. Oyobe, and K. Nakamura, "Efficient optical amplifier using a low-concentration Erbium-doped fiber," *IEEE Photon. Technol. Lett.,* vol. 2, pp. 559–561, Aug. 1990.

[6] M. Shimizu, M. Yamada, M. Horiguchi, and E. Sugita, "Concentration effect on optical amplification characteristics of Er-doped silica single-mode fibers," *IEEE Photon. Technol. Lett.*, vol. 2, pp. 43–45, Jan. 1990.
[7] M. J. F. Digonnet, M. K. Davis, and R. H. Pantell, "Rate equations for clusters in rare earth-doped fibers," *Opt. Fiber Technol.*, vol. 1, pp. 48–58, 1994.
[8] J. Nilsson, P. Blixt, B. Jaskorzynska, and J. Babonas, "Evaluation of parasitic upconversion mechanisms in Er^{3+}-doped silica-glass fibers by analysis of flourescence at 980 nm," *J. Lightwave Technol.*, vol. 13, pp. 341–349, Mar. 1995.
[9] R. S. Quimby, W. J. Miniscalco, and B. Thompson, "Clustering in Erbium-doped silica glass fibers analyzed using 980 nm excited-state absorption," *J. Appl. Phys.*, vol. 76, no. 8, pp. 4472–4478, 1994.
[10] P. Myslinski, J. Fraser, and J. Chrostowski, "Nanosecond kinetics of upconversion process in EDF and its effect on EDFA performance," in *Optical Amplifiers and Their Applications, Proc. OAA'95*, 1995, pp. 100–103, paper ThE3.
[11] P. Blixt, J. Nilsson, Carlnas, and B. Jaskorzynska, "Concentration-dependent upconversion in Er^{3+}-doped fiber amplifiers: Experiments and modeling," *IEEE Photon. Technol. Lett.*, vol. 3, pp. 996–998, Nov. 1991.
[12] F. Di Pasquale, M. Zoboli, M. Federighi, and I. Massarek, "Finite-element modeling of silica waveguide amplifiers with high Erbium concentration," *IEEE J. Quantum Electron.*, vol. 30, pp. 1277–1282, May 1994.
[13] J. L. Philipsen and A. Bjarklev, "Monte Carlo simulations of homogeneous upconversion in Erbium-doped silica glasses," *IEEE J. Quantum Electron.*, vol. 33, pp. 845–854, May 1997.
[14] J. L. Philipsen, J. Broeng, A. Bjarklev, J. E. Pedersen, and B. Pálsdóttir, "Comparison of cluster models in the interpretation of green fluorescence experiment performed on 6 high concentration Erbium-doped silica fibers," in *Optical Amplifiers and Their Applications, Proc. OAA*, 1996, vol. 5, pp. 142–147.
[15] B. Pálsdóttir and C. C. Larsen, "Dipole-dipole model for upconversion and flourescence lifetime in Erbium doped fibers," in *Optical Amplifiers and Their Applications, Proc. OAA'94*, 1994, vol. 14, pp. 83–85, paper ThB5.
[16] P. F. Wysocki, J. L. Wagener, M. J. F. Digonnet, and H. J. Shaw, "Evidence and modeling of paired ions and other loss mechanisms in Erbium-doped silica fibers," *Proc. SPIE*, vol. 1789, pp. 66–79, 1992.
[17] W. Q. Shi, M. Bass, and M. Birnbaum, "Effects of energy transfer among Er^{3+} ions on the flourescence decay and lasing properties of heavily doped $Er:Y_3Al_5O_{12}$," *J. Opt. Soc. Amer. B*, vol. 7, no. 8, pp. 1456–1462, 1990.
[18] A. Bjarklev, *Optical Fiber Amplifiers: Design and System Applications*, 1st ed. Boston, MA: Artech House, 1993.
[19] M. A. Marcus and A. Polman, "Local structure around Er in silica and sodium silicate glasses," *J. Non-Crystalline Solids*, vol. 136, pp. 260–265, 1991.
[20] P. M. Peters and S. N. Houde-Walter, "X-ray absorption fine structure determination of the local environment of Er^{3+} in glass," *Appl. Phys. Lett.*, vol. 70, no. 5, pp. 541–543, 1997.
[21] D. L. Dexter, "A theory of sensitized luminescence in solids," *J. Chem. Phys.*, vol. 21, no. 5, pp. 836–850, 1953.
[22] E. Desurvire, *Erbium Doped Amplifiers: Principals and Applications*, 1st ed. New York: Wiley, 1994.
[23] J. Philipsen, P. Gastaldo, C. Cassagnettes, D. Barbier, A. Kevorkian, and A. Yeniay, "Self-referenced Q-switched pump-probe transmission experiment for the determination of the degree of clustering in Er-doped planar waveguides," in *Optical Amplifiers and Their Applications, Proc. OAA'99*, 1999, paper FC4.

Jacob L. Philipsen was born in Copenhagen, Denmark, on November 22, 1972. He received the M.Sc.E. and Ph.D. degrees from the Technical University of Denmark in 1995 and 1999, respectively. The topic of the Ph.D. work was highly erbium-doped glasses and photonic components. The work was carried out at the Research Center COM at the Technical University of Denmark and during research stays at the Laboratory of Photonics and Microwave Engineering, the Royal Institute of Technology, Stockholm, Sweden, and at the Groupement d'Electromagnetisme Exprimental et d'Optolectronique (GeeO), Grenoble, France.

Since June 1999, he works as an R&D Engineer at Teem Photonics, Grenoble, France, on the development of erbium-doped planar waveguide amplifiers and on their integration with passive integrated photonic components.

J. Broeng, photograph and biography not available at the time of publication.

A. Bjarklev, photograph and biography not available at the time of publication.

Sten Helmfrid was born on July 6, 1963 in Stockholm, Sweden. He received the M. Sc. and Ph.D. degrees from the Royal Institute of Technology, Stockholm, Sweden, in 1987 and 1991, respectively.

In 1991–1992, he worked as a Visiting Scientist on short-wavelength compact light sources at Hitachi Central Research Laboratory, Kokubunji, Japan, and, in the following year and a half, he performed post-doctoral work at the Max-Planck Institute of Quantum Optics, Garching, Germany, where he studied resonance fluorescence from single ions. In 1994, he returned to Sweden and joined the Royal Institute of Technology, first with the Department of Physics II and, since 1995, with the Laboratory of Photonics and Microwave Engineering. Since April 1999, he is a Research Scientist at ACREO AB, a fusion of the industrial research institutes Institute of Optical Research and Industrial Microelectronics Center. His research interests are nonlinear optics, integrated optics, fiber optics, and quantum optics.

Dan Bremberg was born in Danderyd, Sweden, on December 17, 1968. He received the M.Sc. degree in engineering physic and the techn licentiate degree (with the title "Experimental Investigation of energy transfer upconversion in densely Er^{3+} doped silica fibres") from the Department of Electronics, Royal Institute of Technology, Stockholm, Sweden, in 1996 and 1999, respectively.

He is currently employed as a Design Engineer with the Research and Development Department at Nokia Telecommunications, Kista, Sweden.

B. Jaskorzynska, photograph and biography not available at the time of publication.

B. Pálsdóttir, photograph and biography not available at the time of publication.